Nuclear Instruments and Methods in Physics Research B28 (1987) 175–184
North-Holland, Amsterdam

APPLICATIONS OF THE MONTE CARLO CODE TRIPOS TO SURFACE AND BULK ION TRANSPORT PROBLEMS *

P.S. CHOU and N.M. GHONIEM

Mechanical, Aerospace and Nuclear Engineering Department University of California, Los Angeles, California 90024, USA

Received 6 January 1987 and in revised form 30 March 1987

A general dynamic Monte Carlo ion transport code, TRIPOS (TRansport of Ions in POlyatomic Solids) is used in this work. The TRIPOS code uses both power-law cross sections and a newly developed solution to the scattering integral for treatment of large-angle nuclear collisions. Small-angle nuclear collisions and electronic stopping are described as a continuous energy loss in between large-angle ion–atom collisions. Applications of TRIPOS to surface, bulk, and deep penetration problems in multilayer polyatomic media are given.

1. Introduction and background

A sound understanding of the physical phenomena associated with ion transport in solids is critical to the advancement of new and emerging technologies. For example, the first wall and divertor or limiter components of fusion energy devices experience high fluxes of charged particles and neutrons, which lead to a variety of effects (i.e., sputtering, blistering, and bulk damage). The production of primary knock-on atoms (PKAs) in fission nuclear reactor materials leads eventually to the degradation of design and safety-related material properties. New material processing technologies using ion beams or plasmas rely on a detailed knowledge of ion transport physics. Understanding of the physics of radiation damage in structural solids and microelectronic materials is critical to the development of space and defense related technologies.

Ion slowing-down processes can be attributed to ion energy losses through different interactions (e.g., excitation and ionization of electrons, inelastic nuclear collisions, elastic nuclear interactions, and bremsstrahlung photon emissions). There are two general classes of approaches for the analysis of ion transport phenomena, the deterministic and probabilistic methods. Deterministic approaches are based on either analytical or numerical solutions to the ion transport equation. On the other hand, probabilistic solutions rely on using the Monte Carlo method, where an ensemble of particles is used to simulate the ion interaction processes following physical laws.

The ion transport equation is derived based on particle and energy conservation principles [1–6]. The transport equation is quite complex, and analytical or standard discrete numerical solutions for general geometries and a large number of degrees of freedom are non-existent. In polyatomic solids, coupled transport equations are required [5,6] which further increase the complexity of analytical or numerical solutions of the problem. However, if a few ion parameters are desired, simplified forms of the ion transport equation can be used. Lindhard, Scharff, and Schiøtt [7] used the moments method by assuming continuous slowing-down processes to calculate the range distribution and associated parameters. Lindhard et al. [8] developed an integral equation relating radiation damage to deposited energy and atomic displacement. Parking and Coulter [9] extended the treatment for the atomic displacement calculation in polyatomic solids. However, these calculations neglect the spatial distribution of radiation damage.

Sanders [10] derived a vector range distribution function. For one-dimensional geometry, Sigmund [11] expanded the vector range distribution in Legendre polynomials in moment solutions. Brice [12] developed an integral equation describing the energy deposition profiles using a similar approach. All of the above methods, however, use simplified forms of the ion transport equation where detailed particle phase-space are not included. Hoffman et al. [5] used the discrete-ordinate multi-energy-group method, which was originally developed for neutron transport [13,14], for the analysis of surface sputtering problems. Using approximate coupled diffusion equations, Chou and Ghoniem [6] devel-

* This work is supported by the National Science Foundation, Grant #CPE-81-11581; the US Department of Energy, Office of Fusion Energy, Grant #DEFG-3-84ER52110 with UCLA; and te State of California through the MICRO Project, Grant #UC-85-151 with matching funds from TRW Corporation, Grant #TRW-A576778AB5S.

oped an analytical method for the slowing down of ion-induced cascades in precipitate dissolution problems. The diffusion equations were de-coupled using the Neumann series expansion technique.

To describe the many-body interaction of N atoms in the crystal, $3N$ Newtonian equations of motion are required for the description of the crystal. A PKA event can be initiated by giving an atom a kinetic energy E with the momentum gained in a specified direction. Numerical procedure is then used to integrate these equations of motion until equilibrium is reached. These calculations are fully dynamic since all degrees of freedom are allowed to vary simultaneously to satisfy the requirements of interaction forces and the Newtonian laws of dynamics. This many-body integration method is very useful in demonstrating directional effects such as focusing and channeling. The major limitations lie with the maximum available memory capacity and computation speed of a computer. Consequently, only a small number of low energy PKAs can be simulated in this type of analysis [15]. This method is generally referred to as molecular dynamics (MD); the MARLOWE code [16,17] is an example of an MD code.

At PKA energies above few hundred eV, a simplified approximation can be made. Instead of the many-body interaction problem, the ion–atom interaction is treated as a binary collision approximation (BCA). The Monte Carlo method is used within the framework of the BCA. The Monte Carlo method can accurately simulate particle behavior in solids, with modest increments in computational difficulties for each added degree of freedom. This method is particularly suitable for applications of "supercomputers." In the Monte Carlo method, sampling is conducted from probability distribution functions according to relevant physical laws.

Beeler [18,19] applied the assumption that the atomic collision cascade can be described as a branching sequence of binary collision events to ion transport calculations. Yoshida [20], Oen and Robinson [16,17], Ishitani et al. [21], Robinson and Agamy [22], Biersack and Haggmark [23], Ziegler et al. [24]. Attaya [25], and Chou and Ghoniem [26] developed Monte Carlo codes based on the binary collision approximation. Roush et al. [27] as well as Moeller and Eckstein [28] used the same concept to develop time-dependent Monte Carlo codes. In this work, a dynamic binary collision Monte Carlo ion transport code, TRIPOS, is presented. It is a general purpose code for the efficient calculation of ion transport and effects in a multi-layered structure composed of polyatomic solids. TRIPOS can be applied to the analysis of bulk or surface time- and fluence-dependent problems. Thus, complex surface evolution problems can be analyzed. Importance sampling techniques are incorporated in order to enhance the computation speed and reduce the variance in the results.

The validity of the results from ion transport simulations depends heavily on the ability to accurately describe both the interatomic collisional behavior and the electronic energy loss. In order to correctly predict the ion collisional behavior in solids, the interatomic potential has to be known with great accuracy. However, the overlapping and shielding effects of the electron clouds during the atomic collision process make a complete delineation of the interatomic potential difficult. Many interatomic potential models were proposed in the literature. Models most widely used include the Thomas–Fermi [29,30], Bohr [31], Born–Mayer [32], Molière [33], and Ziegler [24] potentials. However, these complex potentials result in difficulties for analytical solutions of the scattering integral. Biersack et al. [23,24] used a fitting function to the numerical results from the scattering integral to approximate atomic scattering. In the present work, two methods of calculating scattering properties are used. The first is based in approximate power-law fits to the Thomas–Fermi potential. In the second method developed by Blanchard, Ghoniem, and Chou (BGC) [34], a second order Taylor expansion about the distance of closest approach is used for the integrand of the scattering integral resulting in accurate analytical solutions.

2. Theoretical background for the TRIPOS code

In this section, we present a brief review of the theoretical background for the TRIPOS code. The interested reader should consult ref. [26] for more detail. Several new theoretical features have been implemented in the code since the original work [26] and their features are discussed in this section.

2.1. Brief description of previous theoretical features

Lindhard et al. [7] used the momentum approximation to solve for the scattering integral based on the power-law potentials. The solutions from the power potentials are applied to the derivation of the so-called power-law cross sections. This technique bypasses the slow and costly process of numerically solving the scattering integral. In the power-law approximation, the differential cross section is given by [35]

$$\mathrm{d}\sigma(E, T) = C_m E^{-m} T^{-1-m}\,\mathrm{d}T, \tag{1}$$

where C_m is a constant and dependent on the ion–target combination and the energy regime. The total nuclear scattering cross section is expressed in the form:

$$\sigma(E) = \frac{C_m}{m} E^{-m}\left[T_s^{-m} - (\Lambda E)^{-m}\right], \qquad m \neq 0, \tag{2}$$

$$= C_0 \ln(\Lambda E/T_s), \qquad m = 0, \tag{3}$$

where Λ is the maximum fractional energy transferred in a collision, and T_s is the lowest energy transferred. At

high energies this characteristic energy, T_s, is taken to be either the surface binding energy or the displacement threshold energy, depending on the application. However, for cases when the total cross section is so large that the mean-free path is less than a lattice constant, a mean-free path of one lattice constant is assumed. The cross section corresponding to a mean-free path of one lattice constant is $\sigma_0 = \pi r_0^2$, where r_0 is one half of the lattice constant. Eqs. (2) and (3) are used to solve for T_s using σ_0. This procedure is also used for the cases where the mean-free path is excessively large to alleviate the erroneous accounting of electronic and small energy nuclear losses.

The free path between nuclear collisions can be sampled from an exponential distribution based on the total cross section. However, if the free path is smaller than r_0, no sampling is used and the mean-free path is employed instead. This conserves the free path distribution, on the average, and does not violate the BCA. The collision probability of an incident ion with one type of polyatomic specie is proportional to both the atomic density and the microscopic scattering cross section of that specie. The scattering angles of the incident ion and a recoil are related to the energy transferred in a collision. The scattering of ions from background atoms is significant. For collisions with background electrons, however, the momentum exchange is so small that the trajectories for ions are not affected. The energy loss of an incident ion resulting from the interaction with electrons can be adequately treated using an electronic stopping power equation that combines the Lindhard–Scharff formula at low energy and Bethe–Bloch equations at high energy [23,24]. In the intermediate energy range, the equation is consistent with experimental observations.

To conserve the total nuclear energy loss, the contribution of small-angle nuclear collisions (i.e., energy transfer less than T_s) has to be considered. A small-angle nuclear stopping cross section is used to take account of the low energy nuclear collisions. It has the form:

$$S_{ns}(E) = \int_{T_c}^{T_s} T \, d\sigma,$$

$$S_{ns}(E) = \frac{C_m}{(1-m)} E^{-m}\left(T_s^{1-m} - T_c^{1-m}\right), \quad m \neq 1, \quad (4)$$

$$S_{ns}(E) = \frac{C_1}{E} \ln\left(\frac{T_s}{T_c}\right), \quad m = 1, \quad (5)$$

where T_c is a cutoff energy of the order of a few eVs. For the case when T_s is less than T_c, the small-angle nuclear stopping cross section is taken to be zero. Therefore, the total "continuous" energy loss, ΔE, has contributions from both electronic stopping as well as small-angle nuclear collision. The energy loss, ΔE, takes the form

$$\Delta E = \Delta l \sum N_i \left[S_e(E) + S_{ns}(E)\right], \quad (6)$$

where S_e is the electronic stopping cross section, N_i the atomic density for the ith specie, and Δl is the free path between "large-angle" nuclear collisions.

2.2. Atomic scattering

Theoretical treatments of atomic scattering in the BCA start with the scattering integral which has the form

$$\theta = \pi - 2\int_{\rho}^{\infty} \frac{p \, dr}{r^2\left[1 - \frac{V(r)}{E_c} - \frac{p^2}{r^2}\right]^{1/2}}, \quad (7)$$

where θ is the deflection angle in the center of mass system, p the impact parameter and ρ the distance of closest approach, E_c the center of mass kinetic energy, and $V(r)$ the interatomic potential. Lindhard et al. [7] used the momentum approximation to simplify the scattering integral. Their approximation for the new scattering integral takes the form

$$\theta = -\frac{1}{E}\frac{d}{dp}\int_0^{\infty} V\left[\left(x^2 + p^2\right)^{1/2}\right] dx, \quad (8)$$

where E is the ion energy in the laboratory system. For power-law potentials with $s = 1$ (pure Coulombic) and $s = 2$, the exact scattering integral can be analytically solved. The results of eq. (8) agree well with those from the exact scattering integral [eq. (7)] for small scattering angles. However, for near head-on collisions, the momentum approximation yields larger scattering angles.

The power-law representations of interatomic potentials are derived from appropriate fits to the Thomas–Fermi potential. Molière [33] and Ziegler et al. [24] have attempted different forms of exponential screening functions to fit interatomic potentials. However, the scattering integral using these potential functions cannot be analytically solved.

The contribution to the deflection angle of the incident ion is considerable when the interacting particles are separated by distances in the vicinity of the point of closest approach; whereas the contribution is negligible when the two particles are separated by larger distances. Based on this concept, Blanchard, Ghoniem, and Chou (BGC) [34] expanded the interaction potential in eq. (7) about the point of closest approach to the second order of a Taylor series expansion. The potential is fully truncated beyond a separation distance of more than a few impact parameters. Analytical solutions of the exact integral [eq. (7)] were obtained for both the Molière and Ziegler potentials.

Fig. 1 shows a comparison between the scattering angle results from the power-law approximation, the BGC analytical solution [34], and exact numerical calculations using Ziegler's universal screening function with dimensionless energies, ϵ, spanning a range of over five

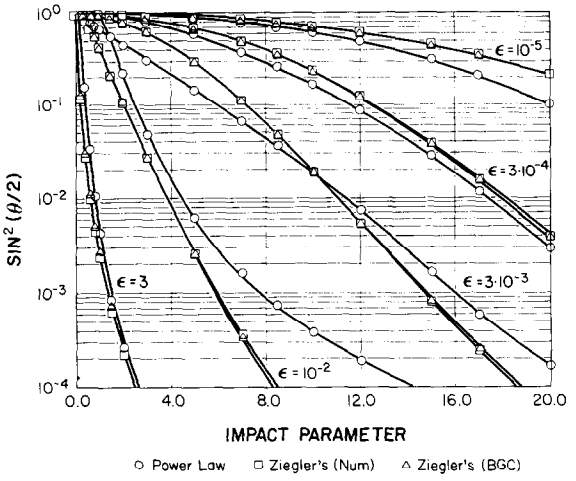

Fig. 1. The scattering angle as a function of impact parameter using power-law and Ziegler's universal potentials at dimensionless energy [eq. (8)] of 10^{-5}, 3×10^{-4}, 3×10^{-3}, 10^{-2} and 3. The scattering integrals are numerically integrated for both power-law and Ziegler's universal potentials. The approximate integral method by BGC [34] is also used to solve for Ziegler's universal potential.

orders of magnitude. Calculations were also made using the Molière potential [34]. The results show the following.

(1) The "exact" form of the screening function has the most significant effect on the solution of scattering integral. This is clear when we compare Molière potential results to calculations with Ziegler's universal potential.
(2) The power law is a reasonable approximation to the scattering process. Its major advantage lies in its simplicity within the context of the Monte Carlo method.
(3) The BGC analytical solution is accurate and within a few percent of the numerical results with impact parameter up to 25 screening lengths for both the Molière and Ziegler potentials.

Because of the relative simplicity of the power-law potential results and the fact that collisions are near-Coulombic at high energies, the majority of the calculations in TRIPOS are performed in this mode. However, for verification, an option using the BGC method is provided.

2.3. Particle history termination and sputtering

A particle history is terminated in two cases: (1) if its energy falls below a minimum value, which is the displacement threshold energy (E_d) in the bulk, or the surface binding energy near the surface; or (2) if it physically leaves the region of interest.

Calculations of sputtering into vacuum are sensitive to the surface binding energy. In this work, the planar potential barrier model is used for slab geometry. The binding energy U at an ejection direction cosine with plane normal μ as in the planar model is given by [27]:

$$U(\mu) = U_0/\mu^2, \tag{9}$$

where U_0 is the minimum energy for particle history termination. For spherical geometry, the isotropic model [11,27] is used,

$$U(\mu) = U_0. \tag{10}$$

To account for all sputtered particles, ions with energy greater than U_0 are simulated. However, it is known that recoils with energy less than the displacement threshold energy are not permanently displaced from their original lattice positions. Cascade simulations by Heinish [36] using the MARLOWE code [16,17] indicated that a displaced atom has to be at least a distance of 6.5 lattice constants away from the vacancy site to be permanently displaced. Based on this conclusion, we define an equivalent surface binding energy, U_{0e}, as follows:

$$\begin{aligned} U_{0e} &= U_0 + x(E_d - U_0)/\lambda \quad && \text{for } x < \lambda, \\ &= E_d, && \text{for } x > \lambda, \end{aligned} \tag{11}$$

where E_d is the displacement energy, x is the depth of recoil generation, and λ is a distance of 6.5 lattice constants. The use of this equivalent surface binding energy results in termination of all bulk recoils with energy less than E_d. This can greatly reduce the number of simulated recoils without affecting the displacement damage or sputtering results.

2.4. Dynamic surface evolution

The evolution of an alloy surface is both time and flux dependent because of the ion beam induced changes in surface compositions. In the TRIPOS code, the surface regions are divided into many layers, the thickness of each being a small fraction of the incident ion projected range. For each layer, atomic species conservation is required to trace time and fluence dependencies. During the simulation, pseudo particle histories are used with each history representing a fluence of W, which is on the order of 10^{12} cm^{-2}. Each layer is generally represented by N pseudo-particles. Conservation requires that

$$N = n\Delta t/W \tag{12}$$

for each layer, where n is the atomic density and Δt is the thickness of the layer. Particle balance is performed for each layer in the events of sputtering, dissolution, and implantation. Such balance yields information on the local layer composition. Also, other phenomena in dynamic surface evolution processes require additional modeling. For example, the recoil implantation and mixing can cause the formation of local superdense material which eventually leads to local relaxation and

expansion. This process is related to the phenomenon of recoil mixing. The superdense solid is modeled to expand homogeneously until the theoretical density is reached.

2.5. Variance reduction and importance sampling

The standard deviation, which is the square root of the variance, is used as a measure of the statistical uncertainty in the Monte Carlo results. The variance decreases with the number of simulated histories. The uncertainty in simulated average results decreases with the square root of the number of particle histories used. Since the cost of computation can be approximately regarded as a linear function of the number of histories, estimates of average values improve moderately with an increase in the number of histories.

Variance reduction techniques can serve as a means to reduce the variance by using complex biased sampling schemes [37–40]. In the meantime, the extra computational efforts which arise because of more complex schemes are counterbalanced by the faster reduction in variance. As a result, the overall cost of computation is reduced, or stays at the same level, while the variance is reduced.

One of the most widely used schemes in variance reduction is called "importance sampling." As implied in its name, importance sampling refers to recording more samples from the more important regions in a given problem. In other words, the regions which are likely to contribute to the final results are well sampled.

In this work, importance sampling is performed using the particle splitting technique. It is desirable to increase the number of histories in important regions to reduce error in the results. The particle splitting techniques splits one particle into several particles with conservation of the total weight (importance) in the important region. This technique artificially increases the number of particles in the important region. Let there be an important region where, once a particle enters, it is split into n particles. The importance of the incoming particle is I_0. Then, the importance for the newly formed particles, I_n, is given by

$$I_n = I_0/n. \tag{13}$$

Through this scheme, the importance of the entire system is conserved. Now, when those split particles leave the important region, it is necessary to reduce the number of particle histories in order to decrease the computation overhead. The Russian roulette scheme is used to reduce the number of particle histories in the less important regions. Let I_0 be the current particle importance and I_n be the desired importance in the less important region, where $I_0 < I_n$. A random number r is called. If $r \leq I_0/I_n$, then the particle survives and its importance is increased from I_0 to I_n. On the other hand, for $r > I_0/I_n$, the particle is eliminated and discarded from further consideration. Statistically, this technique also conserves the importance of the entire system [37–40].

3. Results

Several applications of TRIPOS have been previously reported [26,41]. These include particle and energy reflection [26], precipitate dissolution [26], cascade simulations [41], and low-energy particle-range calculations [26]. In the following, we present applications of TRIPOS to sputtering, dynamic surface evolution, and high-energy deep penetration. A number of examples demonstrate the versatility and capability of the TRIPOS code. We first discuss four examples of surface sputtering. This is followed by an example of deep penetration by high energy protons, and finally surface evolution simulations using the dynamic version of TRIPOS.

Surface sputtering is classified into physical and chemical sputtering. Physical sputtering is caused by the collisional mechanism of the ion–solid interaction, where recoils are energetic enough to reach the surface and overcome the surface binding potentials. On the other hand, chemical sputtering results from the chemical interaction of incident ions with the solids such that new compounds are formed in the surface regions. These newly formed compounds may experience lower surface binding potential barriers. Since TRIPOS is based on the physics of atomic collisions, its applications are limited to the physical sputtering phenomenon.

Sputtering mechanisms are very complex and can be categorized into three regimes: the single knock-on regime, the linear cascade regime, and the spike regime. For the single knock-on regime, the incident ion transfer its energy to target atoms which are ejected through the surface after having undergone a small number of collisions. In the linear cascade regime, recoil atoms are energetic enough to produce higher order recoils with some of them sputtered. The spike regime has a very high density of recoils where nonlinear effects, such as cascade overlap, play a major role in enhancing the sputtering rate. Light ion sputtering generally falls in the single knock-on and linear cascade regimes.

Sputtering erosion rate is measured using the sputtering yield which is defined as the ratio of the sputtered ion flux to the incident ion flux. Monte Carlo simulations have been performed on four different MFECC [Magnetic Fusion Energy Computer Center (at Livermore, CA, USA)] supercomputers, namely, CDC 7600, Cray-1, Cray-1S and Cray-XMP with relative computing speed factors of 0.55, 1.0, 1.0, and 1.3, respectively [42]. In this work, all the CPU time results are normalized with respect to Cray-1.

3.1. Sputtering

3.1.1. ^{4}He on gold and copper

Both TRIM [23] and TRIPOS codes are used to simulate the sputtering caused by ^{4}He ion incident on Cu and Au, where the direction of incidence is normal to the surface. Four-thousand particle histories are used for each calculation. The surface binding energies are 3.5 and 3.8 eV for copper and gold surfaces, respectively [43]. Fig. 2 shows a comparison of sputtering yield results from TRIM and TRIPOS as a function of incident ion energy on the gold surface. Also included for comparison are the experimental data of Bay et al. [44]. Fig. 3 shows theoretical sputtering yield data from TRIM and TRIPOS compared to experimental data by Rosenberg et al. [45] and Yonts [46] on the copper surface. TRIPOS is shown to agree well with experiments. Fig. 4 shows the projected ranges in gold and copper from both TRIM and TRIPOS which are in good agreement. Fig. 5 presents the normalized CPU times for TRIM and TRIPOS, which shows that TRIPOS is 3 to 10 times faster than TRIM.

3.1.2. D on gold

In this case, sputtering of Au by D ions is considered. Fig. 6 shows good agreement between TRIM and TRIPOS on sputtering yield. Also presented are the experimental data of Bay et al. [44] and Furr et al. [47]. Theoretical results are shown to be in reasonable agreement with these experiments. A comparison of the CPU time in fig. 7 shows that TRIPOS is a factor of 10 faster than TRIM in this case.

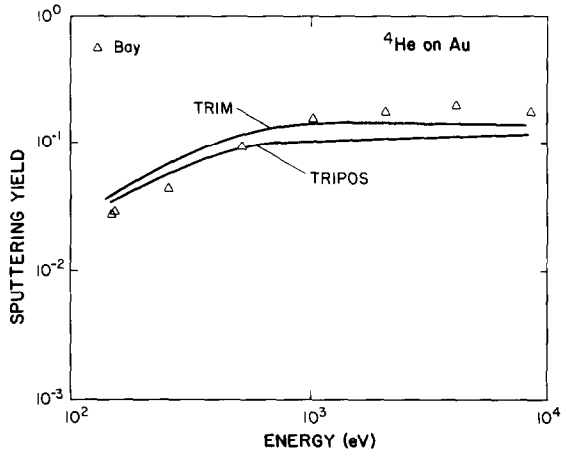

Fig. 2. The sputtering yield as a function of incident ion energies from TRIM, TRIPOS, and experimental results by Bay et al. [44] for α-particles on Au.

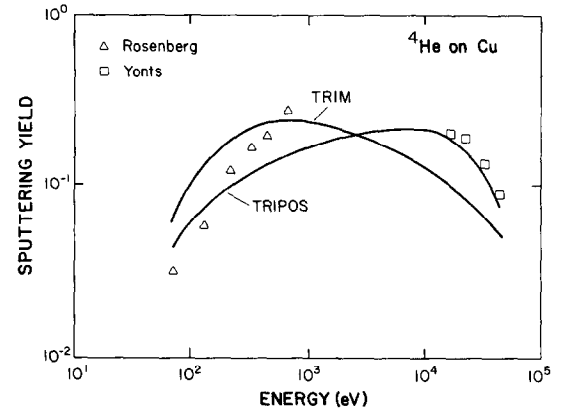

Fig. 3. The sputtering yield as a function of incident ion energies from TRIM, TRIPOS, and experimental results by Rosenberg et al. [45] and Yonts [46] for α-particles on Cu.

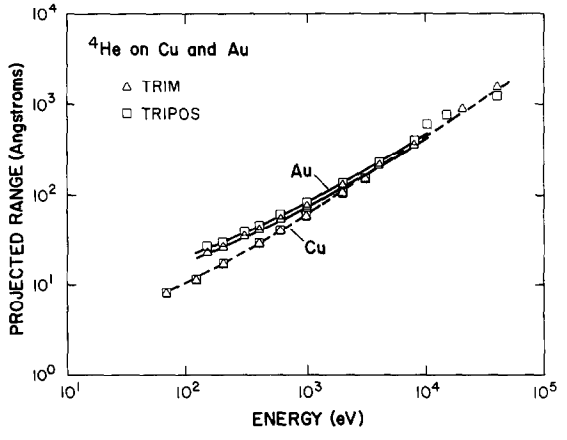

Fig. 4. The projected range predicted by TRIM and TRIPOS as a function of incident ion energies for α-particles on Au and Cu.

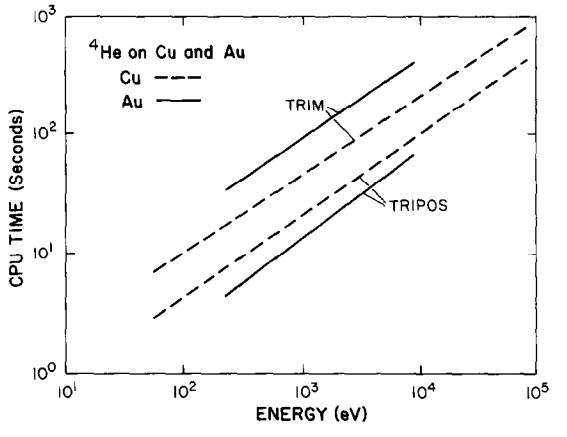

Fig. 5. The normalized CPU time used by TRIM and TRIPOS as a function of incident ion energies for α-particles on Cu and Au. TRIPOS is shown to be 3 and 10 times faster compared to TRIM for Cu and Au, respectively.

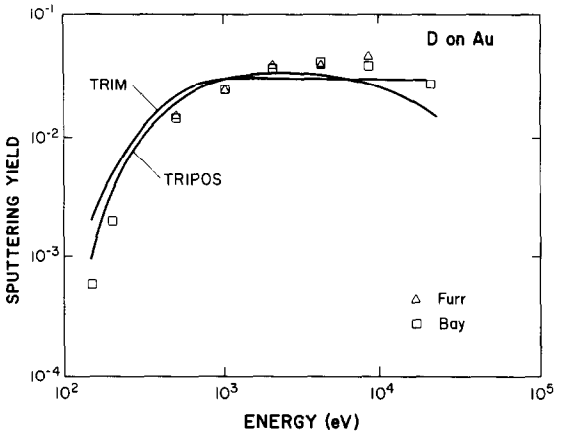

Fig. 6. The sputtering yield as a function of incident ion energies from TRIM, TRIPOS, and experimental results by Bay et al. [44] and Furr et al. [47] for D on Au.

3.1.3. ^{4}He on titanium

The surface binding energy for titanium is taken as 4.9 eV [43]. Based on this binding energy, sputtering yield results from TRIM, TRIPOS, and TRIPOS with the Russian roulette technique of a 4 to 1 kill ratio are obtained. It is observed that the application of Russian roulette in the TRIPOS code yields similar results as compared to analog TRIPOS. Fig. 8 shows a comparison of CPU time used in TRIM, analog TRIPOS, and TRIPOS with the Russian roulette technique. At higher energies, the analog TRIPOS is 10 times faster than TRIM, while the Russian roulette TRIPOS is 30 times faster than TRIM. At low energy, however, the efficiency of the Russian roulette technique decreases because the importance zone thickness is on the order of the projected ion range.

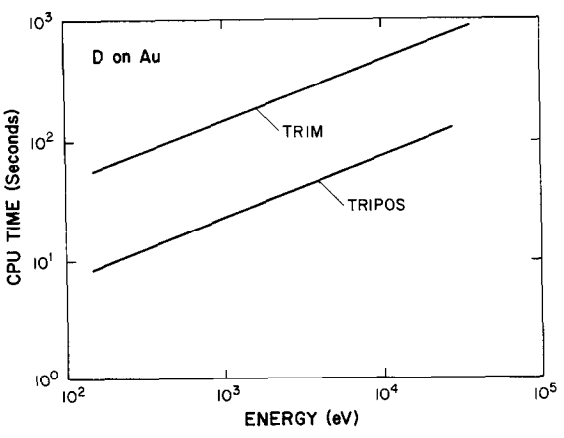

Fig. 7. The CPU time used by TRIM and TRIPOS as a function of incident ion energies for D on Au. TRIPOS is shown to be about 10 times faster than TRIM.

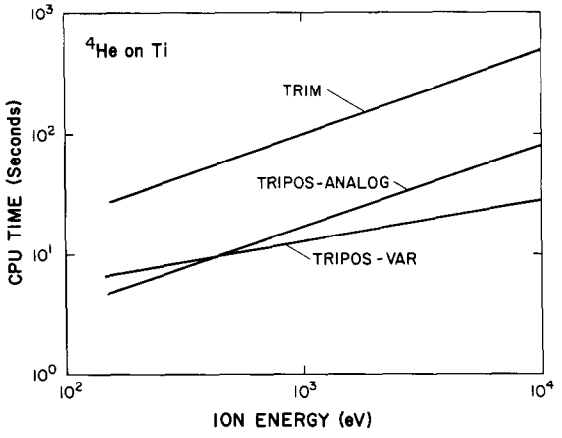

Fig. 8. The CPU time used as a function of incident ion energies by TRIM, TRIPOS (analog), and TRIPOS (variance reduction) for α-particles on Ti. It is shown that the variance reduction technique can be advantageous at higher ion energies. However, the simple scheme of analog Monte Carlo is advantageous at low ion energies.

A comparison of TRIM and TRIPOS sputtering-yield results to the experimental data of Rosenberg et al. [45], Yonts [46], Roth et al. [48], Hofer et al. [49], and Bohdansky et al. [50] shows that both TRIM and TRIPOS overestimate the sputtering yield, using a surface binding energy of 4.9 eV. By increasing the surface binding energy to 7.5 eV, the predictions from the TRIPOS code are more consistent with the experimental data as shown in fig. 9.

3.1.4. ^{4}He on carbon (graphite)

The measured surface binding energy for graphite is 7.4 eV [48]. Predictions of sputtering yield from both

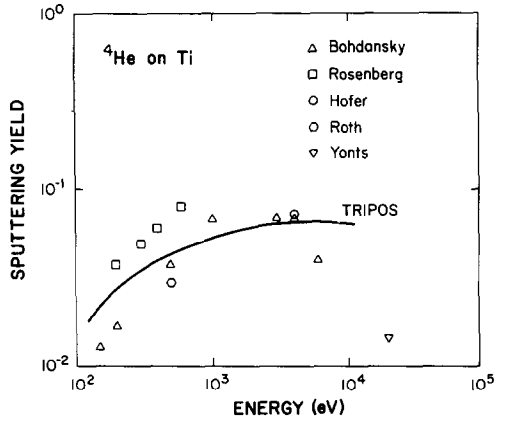

Fig. 9. The sputtering yield from TRIPOS compared to experimental data by Rosenberg et al. [45], Yonts [46], Roth et al. [49], Hofer et al. [50], and Bohdansky et al. [51] as a function of incident ion energy for α-particles on Ti.

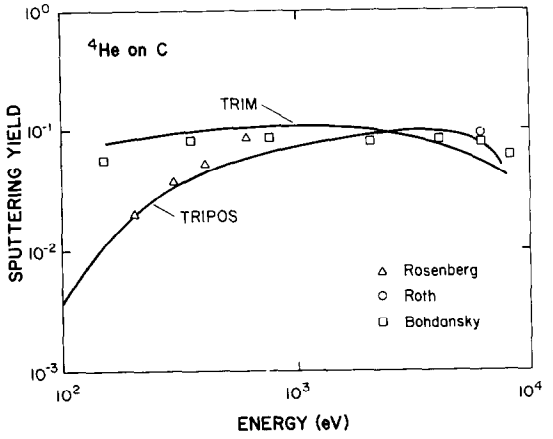

Fig. 10. The sputtering yield from TRIM and TRIPOS compared to experimental results by Rosenberg et al. [45], Bohdansky et al. [52], and Roth et al. [53] as a function of incident ion energy for α-particles on C.

TRIM and TRIPOS show an underestimation of the experimental results by Rosenberg et al. [45], Bohdansky et al. [51], and Roth et al. [52] based on this surface binding energy. A selection of a surface binding energy of 5.0 eV shows a good fit of both TRIM and TRIPOS to the experimental results as shown in fig. 10. Analog TRIPOS simulations were found to be about 6 times faster compared to TRIM in the same figure.

3.2. Deep penetration of protons

In a number of space applications, information on the deep penetration of charged particles is needed. A monoenergetic beam of 200 MeV is considered to be incident on a 9.78-cm-thick aluminum slab. The emerging protons immediately enter a slab of an organic material with the following composition: 27.96% hydrogen, 15.29% carbon, 27.06% nitrogen, and 27.96% oxygen. The projected range calculated by TRIPOS is 13.1 cm. The ion energy deposition along the ion track is shown in fig. 11. The small spikes are caused by high energy PKAs and the dip at 9.78 cm results from the discontinuity in material composition. The range stragglings along the depth (Z-) direction and the X-direction) are shown in fig. 12.

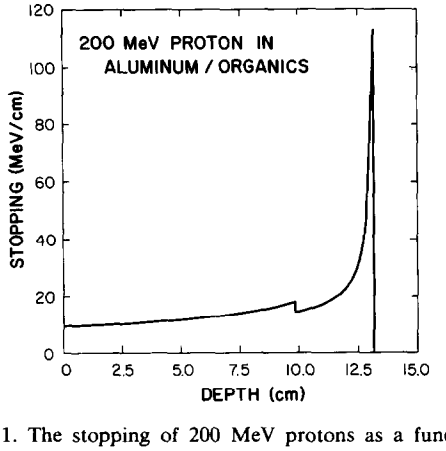

Fig. 11. The stopping of 200 MeV protons as a function of penetration depth in a 9.78-cm-thick aluminum/organic medium. The depth where a discontinuity in the stopping occurs is the boundary for Al and the organic materials.

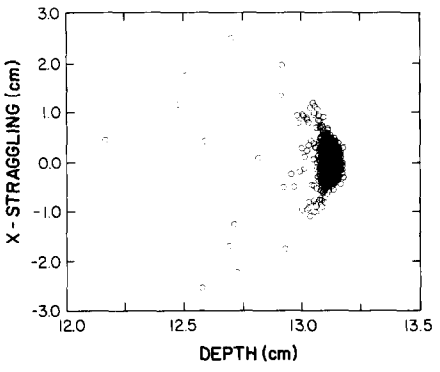

Fig. 12. The straggling of 200 MeV protons along the depth (Z-) direction and the X-direction.

3.3. Dynamic surface evolution

Applications of TRIPOS to dynamic surface evolution problems have been performed on AuPt, LuFe, CuAu, and TiC alloys [53]. TRIPOS showed good agreement with the experimental measurements for 150 eV deuterium ions by Nelson and Bastasz [54] on CuAu for up to a fluence of 5.0×10^{15} particles/cm^2 where gold atom enrichment is observed. TRIPOS results qualitatively agree with the experimental results [55–57] for deuterium and tritium ions on TiC where titanium atom enrichment is observed. Our work shows that the dynamic evolution results depend heavily on the modeling. For a more detailed discussion, the reader is referred to refs. [53] and [58].

4. Conclusions

In this work, diverse varieties of applications of the dynamic Monte Carlo ion transport code, TRIPOS, are presented. The power-law potential approximation to the Thomas–Fermi potentials at high energies and to the Born–Mayer potentials at low energies are used to describe nuclear collisions. Options of using Molière or Ziegler universal potentials are also provided using the integration technique developed by Blanchard, Ghoniem and Chou [34]. Our study shows that the power-law and Born–Mayer potential results agree well with the results from Molière or Ziegler potentials with the exception

that the momentum approximation yield harder collisions at low impact parameters.

It has been shown that both TRIM and TRIPOS give the same order of accuracy in most applications. Limits on the accuracy of both codes are dictated by the treatment of very low energy transfers where the CA breaks down. Because the results are consistent with a large variety of experimental data, this shortcoming is remedied by adjusting the effective surface binding energy and the effective displacement threshold energy. These "effective" values are generally not too far from experimental measurements. The computation speed gained in TRIPOS makes it attractive to treat complicated ion transport problems. This speed is shown to stem from two sources. First, the use of analytical solutions to ion mean-free path and of small-angle nuclear-stopping cross sections allows a significant reduction in the number of simulated atomic collisions. Second, when the analog Monte Carlo scheme is replaced with an importance sampling technique, the total number of particle histories necessary for a desired statistical accuracy is reduced.

TRIPOS simulates ion behavior in materials with multiple layers and different compositions. It treats both surface and bulk ion transport problems where importance sampling techniques are employed. For surface sputtering by light ions, TRIPOS results are in good agreement with the results from both the experiments and the TRIM calculations. Our study shows that analog TRIPOS is a factor of 3 to 10 faster than TRIM. With the Russian roulette technique, TRIPOS can be up to 30 times faster than TRIM. Also, TRIPOS simulations of dynamic surface evolution problems show good agreement with experimental work. However, detailed modeling is still required for a complete description of surface evolution phenomena. One interesting application of TRIPOS is the treatment of deep penetration by energetic ions. This application is useful in the study of single event upset (SEU) phenomena in microelectronic components used in space explorations. A new version of TRIPOS has been developed where coupled ion–electron transport is simulated for semiconductor applications [59].

References

[1] D.E. Bartine, R.G. Alsmiller, F.R. Mynatt, W.W. Engle Jr. and J. Barish, Nucl. Sci. Eng. 48 (1972) 159.
[2] M.M.R. Williams, J. Phys. A9 (1976) 771.
[3] M.M.R. Williams, Radiat. Eff. 37 (1978) 131.
[4] M.M.R. Williams, Progress Nucl. Energy 3 (1978) 1.
[5] J.J. Hoffman, H.L. Dodds and D.K. Holmes, Nucl. Sci. Eng. 68 (1978) 204.
[6] P.S. Chou and N.M. Ghoniem, Nucl. Instr. and Meth. B9 (1985) 209.
[7] J. Lindhard, M. Scharff and H.E. Schiøtt, K. Dan, Vidensk. Selsk. Mat. Fys. Medd. 33 (1963) no. 14.
[8] J. Lindhard, V. Nielsen, M. Scharff and P.V. Thomson, K. Dan. Vidensk. Selsk, Mat. Fys. Medd 33 (1963) no. 10.
[9] D.M. Parkin and C.A. Coulter, J. Nucl. Mater. 85/86 (1979) 611; ibid. 88 (1980) 249; ibid. 95 (1980) 193; ibid. 101 (1981) 261; ibid. 103/104 (1983) 1315; ibid. 117 (1983) 340.
[10] J.B. Sanders, Can. J. Phys. 46 (1968) 455.
[11] P. Sigmund, Phys. Rev. 184 (1969) 383.
[12] D.K. Brice, Appl. Phys. Lett. 16 (1970) 1034; J. Appl. Phys. 46 (1975) 3385.
[13] W.W. Engel, Jr., Radiation Shielding Information Center, Oak Ridge National Laboratory Report CCC-254 (1973).
[14] W.A. Rhoades, D.B. Simpson, R.L. Childs and W.W. Engel, Jr., Radiation Shielding Information Center, Oak Ridge National Laboratory Report CCC-320 (1978).
[15] J.B. Gibson, A.N. Goland, M. Milgram and G.H. Vineyard, Phys. Rev. 120 (1960) 1229.
[16] O. Oen and M.T. Robinson, J. Appl. Phys. 35 (1964) 2515.
[17] O. Oen and M.T. Robinson, Nucl. Instr. and Meth. 132 (1976) 647.
[18] J.R. Beeler and D.G. Besco, J. Appl. Phys. 34 (1963) 2873.
[19] J.R. Beeler, Phys. Rev. 150 (1966) 470.
[20] M. Yoshida, J. Phys. Soc. Jpn. 16 (1961) 44.
[21] T. Ishitani, R. Shimizu and K. Murata, Jpn. J. Appl. Phys. 11 (1972) 125.
[22] J.E. Robinson and S. Agamy, in: Atomic Collisions in Solids, eds., S. Datz, B.R. Appleton and C.D. Moak (Plenum Press, New York, 1975) p. 215.
[23] J.P. Biersack and L.H. Haggmark, Nucl. Instr. and Meth. 174 (1980) 257.
[24] J.F. Ziegler, J.P. Biersack and U. Littmark, The Stopping and Range of Ions in Solids (Pergamon Press, New York, 1985).
[25] H. Attaya, Ph.D. thesis, University of Wisconsin Report UWFDM-420 (1980).
[26] S.P. Chou and N.M. Ghoniem, J. Nucl. Mater. 117 (1983) 55.
[27] M.L. Roush, T.D. Andreadis and O.F. Goktepe, Radiat. Eff. 55 (1981) 119.
[28] W. Moeller and W. Eckstein, Nucl. Instr. and Meth. B2 (1984) 814.
[29] L.R. Thomas, Proc. Cambridge Philos. Soc. 23 (1927) 1.
[30] E. Fermi, Z. Phys. 48 (1929) 73.
[31] N. Bohr, K. Dan. Vidensk. Selsk. Mat. Fys. Medd. 18 (1948) no. 8.
[32] M. Born and J.E. Mayer, Z. Phys. 75 (1932) 1.
[33] G. Molière, Z. Naturforsch A2 (1947) 133.
[34] J. Blanchard, N.M. Ghoniem and S.P. Chou, J. Appl. Phys. 61 (1987) 3120; see also University of California Los Angeles Report ENG-86-41/PPG-1014 (1986) .
[35] K.B. Winterbon, P. Sigmund and J.B. Sanders, K. Dan. Vidensk. Selsk. Mat. Fys. Medd. 37 (1970) no. 14.
[36] H.L. Heinisch, J. Nucl. Mater. 103/104 (1981) 1325.
[37] L.L. Carter and E.D. Cashwell, Particle Transport Simulation with the Monte Carlo Method, TID-26607 (ERDA Tech. Info. Center, Oak Ridge, TN, October 1975).
[38] J.S. Spanier and E.M. Gelbard, Monte Carlo Principles and Tranport Problems (Addison-Wesley, Reading, MA, 1969).

[39] J.M. Hammersley and D.C. Handscomb, Monte Carlo Methods (Wiley and Sons, New York, 1964).
[40] W.E. Selph and C.W. Garrett, in: Reactor Shielding for Nuclear Engineers, ed., N.M. Schaffer, TID-25951 (Nat. Tech. Info. Serv., Springfield, VA, 1983) p. 207.
[41] S.P. Chou and N.M. Ghoniem, J. Nucl. Mater. 137 (1985) 63.
[42] K. Fong, MFECC consultant, private communication (1984).
[43] K.A. Gschneider, Solid State Phys. 16 (1964) 275.
[44] H.L. Bay, J. Roth and J. Bohdansky, J. Appl. Phys. 48 (1977) 4722.
[45] D. Rosenberg and G.K. Wehner, J. Appl. Phys. 33 (1962) 1842.
[46] O.C. Yonts, Proc. Nucl. Fusion Reactor Conf. British Nuclear Society, Culham (1969) p. 424.
[47] A.K. Furr and C.R. Fingeld, J. Appl. Phys. 41 (1970) 1739.
[48] J. Roth, J. Bohdansky and W. Ottenberger, Garching Institute of Plasma Physics Report IPP 9/26 (1979).
[49] W.O. Hofer, H.L. Bay and P.J. Martin, J. Nucl. Mater. 76 (1978) 56.
[50] J. Bohdansky, J. Roth and M.K. Sihha, in: Proc. 9th Symp. on Fusion Technology, Gairnisch (FRG), June 1976 (Pergamon Press, Oxford, 1976) p. 541.
[51] J. Bohdansky, J. Roth and W. Ottenberger, J. Nucl. Mater. 76 (1978) 163.
[52] J. Roth, J. Bohdansky and W. Poschenrider, J. Nucl. Mater. 63 (1976) 222.
[53] S.P. Chou and N.M. Ghoniem, J. Nucl. Mater. 141/143 (1986) 216.
[54] G.L. Nelson and R. Bastasz, J. Vac. Sci. Technol. 20 (1982) 498.
[55] C. Ferro, E. Franconi, A. Neri and F. Brossa, J. Nucl. Mater. 101 (1981) 224.
[56] E. Franconi and C. Ferro, J. Nucl. Mater. 128/129 (1984) 929.
[57] K. Oishi, Y. Kumushiko, A. Fujimore and S. Usami, J. Nucl. Mater. 128/129 (1984) 934.
[58] S.P. Chou, Ph.D. thesis, University of California Los Angeles Report ENG-86-13/PPG-939 (1986).
[59] R. Martin and N.M. Ghoniem, University of California Los Angeles Report ENG-86-46/PPG-1024 (1987). See also Monte Carlo simulation of coupled ion–electron transport in semiconductors, submitted to Phys. Status Solidi A.